# High Fidelity Finite Difference Model for Exploring Multi-DOF Thermoelectric Generator Design Space

Chad A. Baker<sup>a</sup>, Haiyan Fateh<sup>a</sup>, Li Shi<sup>a</sup>, Matthew J. Hall<sup>a</sup>

<sup>a</sup>Mechanical Engineering University of Texas 1 University Station, C2200 Austin, TX 78712

### **Abstract**

stuff

Keywords: thermoelectric, model

### 1. Introduction

One third or more of the energy content of the fuel of a typical diesel engine is expelled through the tailpipe as waste heat, so any amount of waste heat usefully recovered is a benefit to vehicle efficiency Heywood (1988); Caton (2000); Endo et al. (2007). Potential waste heat recovery technologies currently under consideration for automotive applications are organic Rankine cycles Miller et al. (2009), turbo-compounding Weerasinghe et al. (2010), direct usage of the waste heat as thermal energy, powering absorption chillers Talom and Beyene (2009), and thermoelectric (TE) devices Miller et al. (2009); Hendricks (2007); Hendricks and Lustbader (2002); Hussain et al. (2009); Crane (2011); Crane and Jackson (2004); Crane et al. (2001). Thermoelectric devices in particular are appealing for automotive applications in that they do not have moving parts, and thermal energy can be converted into electricity directly. Their high cost and low efficiency are currently issues, but the potential use of relatively inexpensive and abundant element materials such as Mg<sub>2</sub>Si<sub>0.5</sub>Sn<sub>0.5</sub> and MnSi<sub>1.75</sub> for TE devices shows promise for future cost reductions and improved performance Rowe (2006). A schematic of a TE leg pair, which is the most fundamental part of a TE device (a device typically consists of hundreds of leg pairs) is shown in Figure 1.

Email address: calbaker@utexas.edu (Chad A. Baker)

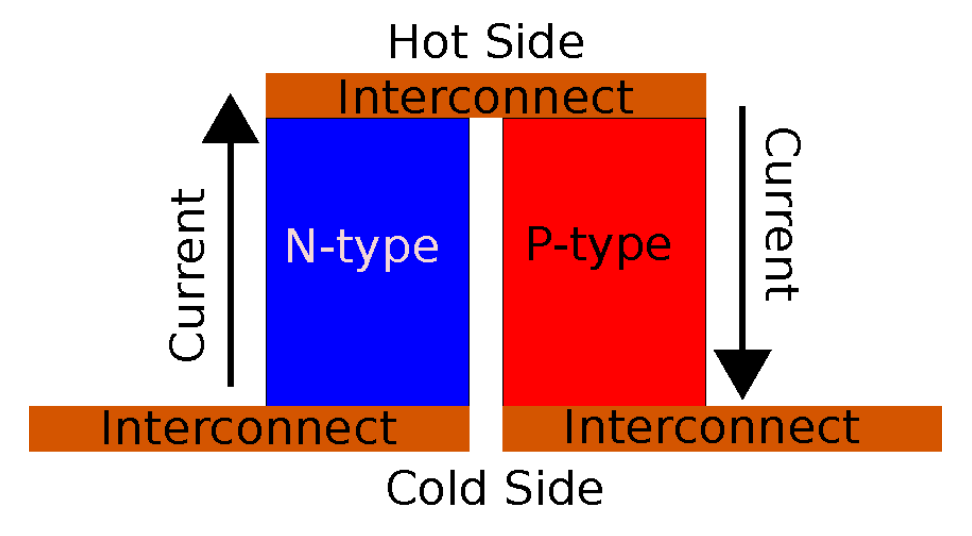


**Figure 1:** Schematic of TE leg pair. A TE leg pair is the smallest unit that can function as a standalone TE device. A typical TE device consists of hundreds of these pairs in series and/or parallel arrangement.

A number of researchers have reported both modeling and experimental work with TE vehicle waste heat recovery with varying emphasis on heat exchanger performance and TE device performance. Stobart and coworkers modeled and experimentally tested TE performance for devices with exhaust temperatures up to 800 K. Because of internal thermoelectric conversion, there is a difference between the hot side and cold side heat transfer of TE devices. This heat transfer asymmetry was not accounted for in the work by Stobart and coworkers. They used an efficiency model based on the average figure of merit (ZT) of the TE material that assumes optimal device geometry and optimal current Stobart and Milner (2009); Stobart et al. (2010). Optimal geometry consists of n-/p-type leg area ratio, leg height, the distance between adjacent legs. Modeling efforts by Hendricks et al. Hendricks and Lustbader (2002); Hendricks (2007) reported using temperature-dependent TE properties (Seebeck coefficient, electrical resistivity, and thermal conductivity) to determine optimal TE leg areas, lengths, and device designs. Miller et al. studied heat transfer and heat exchanger optimization for a combined TE and organic Rankine cycle waste heat recovery system. Miller et al. calculated the TE device efficiency based on an average ZT for state of the art TE materials evaluated at typical operating temperatures Miller et al. (2009). Hussain et al. developed a model with single node TE devices that accounted for transient behavior and thermal asymmetry. In their model, the spatial variation and temperature dependence of the TE properties in individual TE devices were not accounted for. No attempt was made to account for restriction of the exhaust flow in the form of back pressure on the engine Hussain et al. (2009). Back pressure is an important design consideration because the pumping effort the engine must exert to expel exhaust gases is increased if back pressure in the exhaust system is increased. Increased pumping effort takes useful power away from the engine crank shaft.

Crane and coworkers developed a model for cross-flow and counter-flow heat exchanger configurations. They used an analytical, thermally-lumped TE leg performance model that correctly accounted for thermal asymmetry. Some of this modeling work was also validated with experimental results. Crane's most recent model incorporated transient performance Crane et al. (2001); Crane and Jackson (2004); Crane (2011). None of the previous work discussed here used a TE model that accounted for spatial- and temperature-variant properties within the TE material of an individual TE couple.

This dissertation reports a modeling study of TE vehicle waste heat recovery devices based on Mg<sub>2</sub>Si<sub>0.5</sub>Sn<sub>0.5</sub> and MnSi<sub>1.75</sub> materials with consideration of both system level heat exchanger performance and TE device performance. The model presented in this dissertation offers an improvement over existing models because it used a finite difference method to account for spatial- and temperature-variant TE properties at the individual TE leg pair scale. The model also coupled the hot- and cold-side convection heat flux to the TE heat flux, thus accounting for the thermal asymmetry, using a numerical root finding algorithm. This model incorporated back pressure as part of an optimization metric in the form of pumping power requirement. The output of the system model was heat transfer, TE power, pumping power requirement, and the net power output, where the net power output is the total TE power minus the pumping power required to move the coolant and exhaust through the heat exchanger. The model was used to predict overall performance of several heat exchanger systems, incorporating different fin geometries and flow arrangements for enhancing heat transfer and TE power generation. The important TE parameters were optimized using a numerical algorithm, and the optimization metric used by the algorithm was the net power of the system.

This work also includes two generations of TE waste heat recovery systems that were built and tested in the exhaust system of a Cummins 6.7 L turbo Diesel engine. The experimental work was used to validate the model so that the model could be used both as a design tool and a means of thoroughly optimizing various parameters in the TE waste heat recovery system design space.

The first generation TE system consisted of a compact heat exchanger without any TE devices. This system was built to validate the convection heat transfer and flow model using only a small portion of the exhaust flow of the Cummins engine. In order to validate the model at full scale, a second generation TE heat exchanger system was constructed to utilize the entire flow of the Cummins engine. Experimental apparatus, methods, and results from each heat exchanger will be presented separately in Chapters ?? and ??.

A key contribution of this work was recognizing that for almost any practical TE device application, the boundary conditions on the hot and cold side will be convection boundary conditions rather than specified temperature boundary conditions. The TE model developed here accounts for that, and in addition, the model accounts for spatially/thermally variant properties in the direction of heat flow and thermal asymmetry.

# 2. TE Device Testing

This may be beyond the scope.

# 2.1. Steady State

This may be beyond the scope.

#### 2.2. Transient

This may be beyond the scope.

#### 3. Model

#### 3.1. Analytical Model

The TE devices were modeled using Domenicali's energy balance equation and the thermoelectric heat flux equation Domenicali (1953); Hogan and Shih (2006):

$$\frac{d}{dx}\left(k\frac{dT}{dx}\right) = -\rho J^2 + JT\frac{d\alpha}{dx} \tag{1}$$

and

$$q = JT\alpha - k\frac{dT}{dx} \tag{2}$$

where x is the coordinate along the direction of heat and current flux, k is the thermal conductivity, T is the temperature,  $\rho$  is the electrical resistivity, J is the current flux, and  $\alpha$  is the Seebeck coefficient, all evaluated at T.

For completeness, the entire solution for Equations 1 and 2 will be presented here. This solution has been presented in the literature Hogan and Shih (2006) with a critical sign error, and the present work corrects this error.

A tractable solution can be achieved through several steps of algebraic manipulation. First, rearranging Equation 2 yields

$$\frac{dT}{dx} = \frac{JT\alpha - q}{k} \tag{3}$$

This is the final equation for determining the temperature gradient. In order to determine the heat flux gradient, Equation 3 is multiplied by k and substituted into Equation 1, resulting in

$$\frac{d}{dx}(JT\alpha - q) = -\rho J^2 + JT\frac{d\alpha}{dx}$$
(4)

For constant current density (e.g. if the cross-sectional area of the leg is constant), the product rule can be used to expand the left-hand-side to

$$J\left(\frac{dT}{dx}\alpha + \frac{d\alpha}{dx}T\right) - \frac{dq}{dx} = -\rho J^2 + JT\frac{d\alpha}{dx}$$
 (5)

The temperature gradient in first term on the left-hand-side of Equation 5 can be replaced by substituting Equation 3, and after some rearranging, this yields

$$\frac{dq}{dx} = \rho J^2 + J\alpha \frac{JT\alpha - q}{k} \tag{6}$$

Multiplying the second term  $(J\alpha \frac{JT\alpha-q}{k})$  by  $\frac{\rho}{\rho}$  and recognizing the definition of ZT (Equation ??) yields the final result:

$$\frac{dq}{dx} = \rho J^2 \left(1 + ZT\right) - \frac{J\alpha q}{k} \tag{7}$$

Current density, rather than load resistance, is specified in the model. However, it may be desired to specify load resistance for experimental or design purposes. To fully close the model for a specified load resistance, an expression is needed to relate current density to load resistance. This is given by

$$R_{\rm L} = \frac{V_{\rm S,n} - I/A_{\rm n}\rho_{\rm n}l + V_{\rm S,p} - I/A_{\rm p}\rho_{\rm p}l}{I}$$
 (8)

where  $R_{\rm L}$  is the load electrical resistance, l is the length of the TE legs, subscripts n and p indicate n- or p-type leg, and  $V_{\rm S}$  is the Seebeck voltage, given by

$$V_{\rm S} = \sum_{i=1}^{N} \alpha_i \left( T_i - T_{i-1} \right)$$
 (9)

and the current, I, is given by

$$I = JA \tag{10}$$

where J is current density of either leg, and A is the cross-sectional area of either leg. Either leg can be used for this calculation, provided the same leg is used for both the current density and the area. The total power was calculated by

$$\dot{W}_{\rm elec} = IR_{\rm L} \tag{11}$$

where  $\dot{W}_{\rm elec}$  is the electrical power output.

For a pair of thermoelectric legs with convection heat transfer on both sides and isothermal interconnects with no generation, the boundary conditions are combined heat flux and temperature. The interconnects, which are typically copper, are assumed to be isothermal because the thermal conductivity is high. Generation due to Joule heating is assumed to be negligible due to high electrical conductivity, and thermoelectric energy conversion at the interface of the interconnects and the TE materials is neglected. A schematic that will be referenced for both the analytical and numerical finite difference equations is shown in Figure 3. On both the hot and cold side of the TE leg pair, the temperature of each leg must be equal to the temperature of the isothermal interconnect interface, and this is also the temperature driving convection heat flux. The composite heat flux is given by

$$q_{\text{comp}} = \frac{A_{\text{n}}q_{\text{n}} + A_{\text{p}}q_{\text{p}}}{A_{\text{n}} + A_{\text{p}} + A_{\text{void}}}$$
(12)

where A is the cross-sectional area of the n- or p-type leg or that of the void space, and q is the composite heat flux or the heat flux in the specified leg. Subscripts n, p, void, and comp indicate whether the variable references the n-type, p-type, void space, or composite value. A visual representation of the p-type, n-type and void areas is shown in Figure 2. The void area is the empty space between adjacent TE legs, and it is assumed to be perfectly insulated.

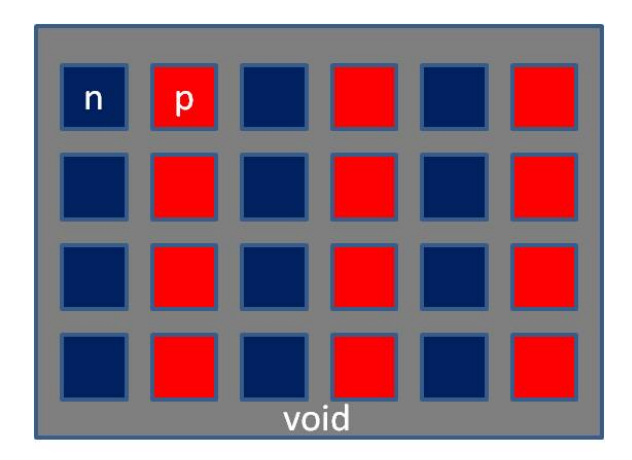


Figure 2: Visual reprentation of p-type, n-type, and void areas.

The composite heat flux must be equal to the convection heat flux on both the hot and cold sides, given by

$$q_{\rm h,comp} = U_{\rm h} \left( T_{\rm h,conv} - T_{\rm h} \right) \tag{13}$$

for the hot side and

$$q_{\rm c,comp} = U_{\rm c} \left( T_{\rm c,conv} - T_{\rm c} \right) \tag{14}$$

for the cold side, where U is the overall heat transfer coefficient for the hot or cold side (including thermal resistance due to conduction and contact resistances associated with the Al plate, substrate, and interconnect shown in Figure 3 as well as thermal resistance due to convection; see Section ??),  $T_{conv}$  is the temperature of the hot or cold fluid, T is the temperature of the hot or cold side of the TE leg pair, and  $q_{comp}$  is the composite heat flux on the hot or cold side of the TE device, given in Equation 12. Subscripts h and c indicate whether the variable corresponds to the hot or cold side. The temperature boundary conditions are specified as follows:

$$T_{\rm n,h} = T_{\rm p,h} = T_{\rm h} \tag{15}$$

$$T_{\rm n,c} = T_{\rm p,c} = T_{\rm c} \tag{16}$$

where, as before, subscripts n and p indicate n- or p-type leg, and subscripts c and h indicate cold or hot side.

# 3.2. Thermoelectric Finite Difference Model

Following the procedure from Hogan and Shih Hogan and Shih (2006), the equations from Section 3.1 can be discretized to the following pair of first order, reverse-

looking finite difference equations:

$$T_{i} = T_{i-1} + \left(\frac{JT_{i-1}\alpha_{i-1} - q_{i-1}}{k_{i-1}}\right)\Delta x \tag{17}$$

from Equation 3, and

$$q_i = q_{i-1} + \left(\rho_{i-1}J^2 + (1 + ZT_{i-1}) - \frac{J\alpha_{i-1}q_{i-1}}{k_{i-1}}\right)\Delta x \tag{18}$$

from Equation 7, where the subscripts i and i-1 indicate the current and previous nodes, respectively, and the TE properties are all evaluated at the temperature of the previous node. A schematic of the system being discretized is shown in Figure 3.

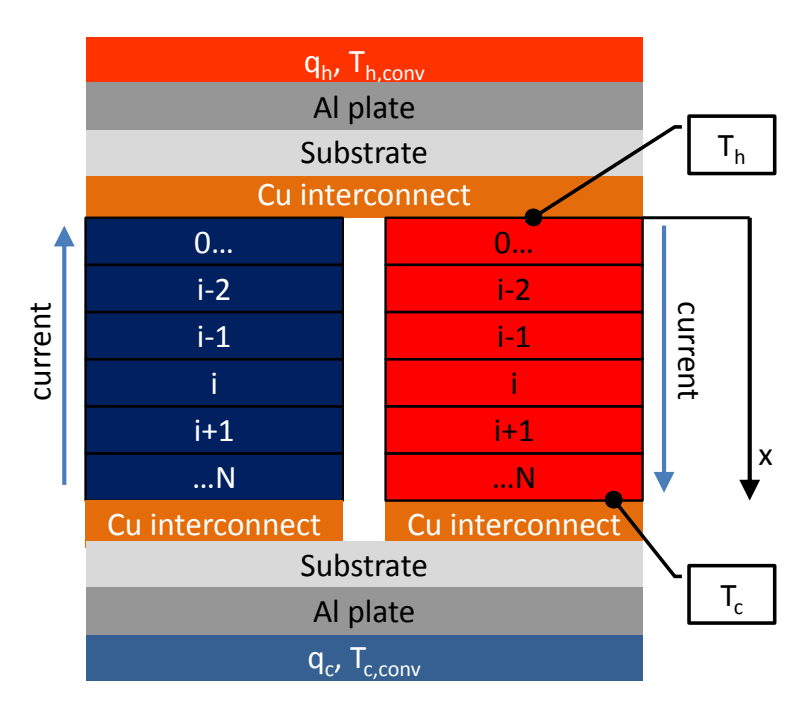


**Figure 3:** Schematic of numerical scheme used to solve TE leg pair. Blue leg is n-type and red leg is p-type.

The algorithm used to solve these coupled finite difference equations deviated substantially from the method described by Hogan and Shih Hogan and Shih (2006) in that the algorithm accounted for a convection (Neumann) boundary condition rather than a temperature (Dirichlet) boundary condition. This is important because

in most practical applications will have temperature-driven heat flux, or convection, boundary conditions. The necessary boundary conditions are fluid temperature and heat transfer coefficient on both the hot and cold side of the TE device as well as the hot and cold side temperature of the TE device. The hot and cold side TE device temperature boundary conditions are satisfied by

$$T_{0,n} = T_{0,n}$$
 (19)

and

$$T_{N,n} = T_{N,p} \tag{20}$$

where subscript 0 indicates the node in contact with the hot side copper interconnect, subscript N indicates the node in contact with the cold side copper interconnect, and the second subscript indicates n-type or p-type TE leg. The heat flux boundary conditions are given by following conditions:

$$U_{\rm h} \left( T_{\rm h,conv} - T_{\rm h} \right) = q_{\rm h,comp} \tag{21}$$

and

$$U_{\rm c} \left( T_{\rm c.conv} - T_{\rm c} \right) = q_{\rm c.comp} \tag{22}$$

The algorithm proceeds as follows:

- 1. Estimate hot side heat flux for the n-type leg, hot side heat flux for the p-type leg, and hot side temperature based on pure conduction and convection.
- 2. Solve for the temperature and heat flux profiles in both the n-type and p-type TE legs using Equations 17 and 18.
- 3. Determine the error between the composite TE heat flux and the convection heat flux (Equations 21 and 22) for both the hot and cold sides.
- 4. Determine the error between the cold side p-type and n-type temperatures, as given by Equations 19 and 20.
- 5. Iterate until the error in steps 3 and 4 is zero.

The iteration was performed by the *fsolve* function of the open source Python 2.7 SciPy package.

- 3.3. Steady State
- 3.3.1. Design Space and Optimization
- 3.4. Transient

This may be beyond the scope.

## 4. Results and Discussion

# 4.1. Steady State

# 4.1.1. Design Space and Optimization

As indicated in Section ??, n-/p-type leg area ratio, leg length, fill fraction, and current (as a surrogate for load resistance) were all used as optimization parameters for maximizing net power output. Optimal n-/p-type leg area ratio remained relatively constant with respect to the other parameters. This is because temperature dependency of the thermoelectric properties exhibited similar trends for both the n- and p-type materials. The latter three parameters, leg length, fill fraction, and current, exhibited some strongly interdependent tendencies in the way they affected power output, and to demonstrate this, surface projections of the 3-dimensional design space are plotted in Figure 4. The optimal values for each parameter in the design space are shown in Table 1. For this design space, n-/p-type leg area ratio is held constant at 0.7 because there is almost no change in optimal leg area as the other parameters are varied. Convection boundary conditions are 300 K and 680 K with overall heat transfer coefficients of 8  $\frac{kW}{m^2K}$  and 2  $\frac{kW}{m^2K}$  for the coolant and exhaust, respectively. These boundary condition are typical values for coolant and exhaust averaged in the stream-wise direction in the model heat exchangers.

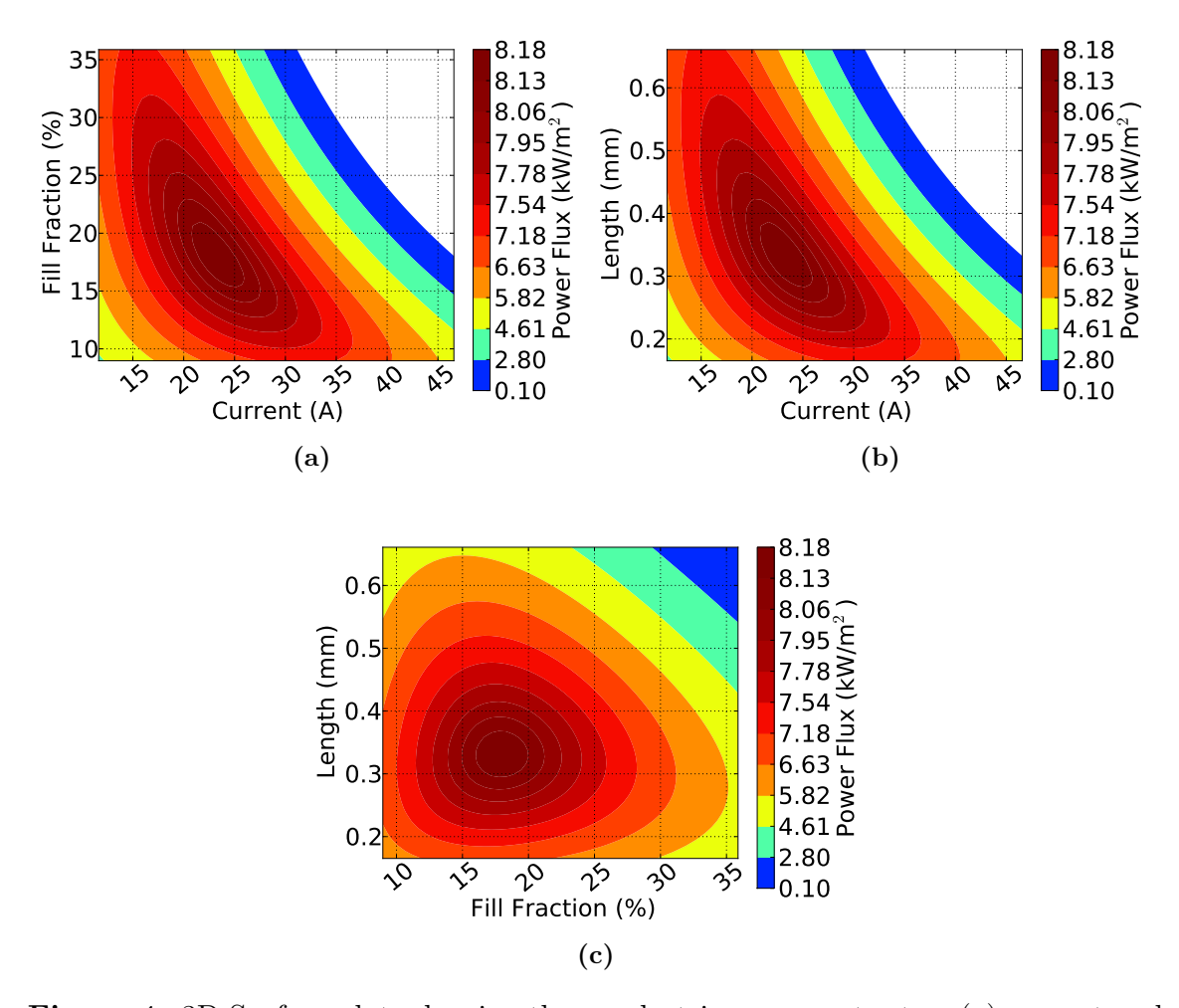


**Figure 4:** 3D Surface plots showing thermoelectric power output v. (a) current and fill fraction, (b) current and length, and (c) fill fraction and length. n-/p-type leg area ratio is held constant at 0.7. Convection boundary conditions are 300 K and 680 K with overall heat transfer coefficients of 8  $\frac{kW}{m^2K}$  and 2  $\frac{kW}{m^2K}$  for the coolant and exhaust, respectively.

**Table 1:** Optimal parameters for design space of standalone TE device, as determined by model. Convection boundary conditions are 300 K and 680 K with overall heat transfer coefficients of 8  $\frac{kW}{m^2K}$  and 2  $\frac{kW}{m^2K}$  for the coolant and exhaust, respectively.

Parameter	Value
fill fraction	17.9 %
leg length	$0.330~\mathrm{mm}$
current	23.3 A
n-/p-type leg area ratio	0.700

These results indicate that changing any of the three variables (fill fraction, leg length, or current) can greatly impact the effect the other two have on performance. This also shows that there is a clearly defined optimal location within the design space. Leg area ratio is included because it does require optimization, but the optimal n-/p-type leg area ratio is insensitive to the other three parameters as well as boundary conditions.

Note that the results presented in Figure 4 vary with convection boundary conditions, and as such, the HX system model would produce results that are somewhat shifted in the design space due to a range of convection boundary conditions throughout the stream-wise direction of the heat exchanger. Exploring this relationship is beyond the scope of the present work.

## 4.2. Transient

This may be beyond the scope.

# 5. Conclusions

# Acknowledgments

- Caton, J.A., 2000. Operating characteristics of a spark-ignition engine using the second law of thermodynamics: effects of speed and load. SAE Technical Paper, 2000–01–0952.
- Crane, D., Jackson, G., Holloway, D., 2001. Towards Optimization of Automotive Waste Heat Recovery Using Thermoelectrics. Technical Report 2001-01-1021. SAE International. Warrendale, PA.
- Crane, D.T., 2011. An introduction to system level steady-state and transient modeling and optimization of HighPower density thermoelectric generator devices made of segmented thermoelectric elements. Journal of Electronic Materials 40, 561–569.
- Crane, D.T., Jackson, G.S., 2004. Optimization of cross flow heat exchangers for thermoelectric waste heat recovery. Energy Conversion and Management 45, 1565–1582.
- Domenicali, C.A., 1953. Irreversible thermodynamics of thermoelectric effects in inhomogeneous, anisotropic media. Physical Review 92, 877–881.
- Endo, T., Kawajiri, S., Kojima, Y., Takahashi, K., Baba, T., Ibaraki, S., Takahashi, T., Shinohara, M., 2007. Study on Maximizing Exergy in Automotive Engines. Technical Report 2007-01-0257. SAE International. Warrendale, PA.
- Hendricks, T.J., 2007. Thermal system interactions in optimizing advanced thermoelectric energy recovery systems. Journal of Energy Resources Technology 129, 223–231.
- Hendricks, T.J., Lustbader, J.A., 2002. Advanced thermoelectric power system investigations for light-duty and heavy duty applications. II, in: Thermoelectrics, IEEE. p. 387–394.
- Heywood, J., 1988. Internal Combustion Engine Fundamentals. McGraw-Hill Science/Engineering/Math. 1 edition.
- Hogan, T.P., Shih, T., 2006. Modeling and characterization of power generation modules based on bulk materials. Boca Raton, FL: CRC Press. Eq. 12.25 contains a typo. Equation 10 in this paper is the correct form.
- Hussain, Q.E., Brigham, D.R., Maranville, C.W., 2009. Thermoelectric Exhaust Heat Recovery for Hybrid Vehicles. Technical Report 2009-01-1327. SAE International. Warrendale, PA.

- Miller, E.W., Hendricks, T.J., Peterson, R.B., 2009. Modeling energy recovery using thermoelectric conversion integrated with an organic rankine bottoming cycle. Journal of Electronic Materials 38, 1206–1213.
- Rowe, D.M., 2006. Thermoelectrics Handbook: Macro to Nano. CRC/Taylor & Francis, Boca Raton.
- Stobart, R., Milner, D., 2009. The Potential for Thermo-Electric Regeneration of Energy in Vehicles. Technical Report 2009-01-1333. SAE International. Warrendale, PA.
- Stobart, R.K., Wijewardane, A., Allen, C., 2010. The Potential for Thermo-Electric Devices in Passenger Vehicle Applications. Technical Report 2010-01-0833. SAE International. Warrendale, PA.
- Talom, H.L., Beyene, A., 2009. Heat recovery from automotive engine. Applied Thermal Engineering 29, 439–444.
- Weerasinghe, W., Stobart, R., Hounsham, S., 2010. Thermal efficiency improvement in high output diesel engines a comparison of a rankine cycle with turbo-compounding. Applied Thermal Engineering 30, 2253–2256.